

PCs that are important for the horizontal VOR. (i) They exhibit modulation of complex-spike firing in relation to retinal image motion away from the side of the recording (16). (ii) Motor learning causes their simple-spike firing to express changes in firing that are in the correct direction to support the altered VOR (17). The simple spike firing of these PCs is modulated preferentially for horizontal rather than vertical pursuit eye movements.

For 34 PCs studied after decreases in the gain of the VOR (18), the response latency during the VOR averaged 21.3 ms. The criterion latency for PCs (vertical dashed line in Fig. 3B) was estimated as 10 ms, which is 2 ms shorter than that for FTNs. This takes account of the latency at which stimulation of the flocculus inhibits FTNs (1 to 2 ms) and of the latency for evoking an eye movement by single shock stimulation of the flocculus (9 to 10 ms) (Fig. 1A). Most PCs responded too late either to contribute to the modified pathways or to cause the modified responses in FTNs (Fig. 3B). However, a few PCs did respond early enough to cause the change in FTN firing. Further experiments will be needed to test the possibility that these few PCs cause motor learning and that the FTNs and the rest of the PCs follow.

FTNs satisfy two criteria established by our earlier work for neurons in the modified pathways. One criterion is based on the fact that unmodified VOR pathways make a fixed contribution to the VOR. Changes in firing in the modified pathways will therefore have to exceed the change in the VOR. FTNs satisfy this criterion: after decreases in the gain of the VOR, eye motion is still opposite in direction to head motion, but FTNs show a reversed response. FTNs also satisfy a second, latency criterion (3): they respond to vestibular stimuli at a latency that is appropriate to be part of the modified pathways. We conclude that FTNs are in the modified VOR pathways. Because FTNs generally respond before PCs, future experiments should evaluate brain stem vestibular inputs to FTNs as a possible site of motor learning.

7. Our methods are detailed in (4) and in S. G. Lisberger and F. A. Miles [*J. Neurophysiol.* **43**, 1725 (1980)].
8. The relation between firing rate and eye position almost always had a "knee" such that the slope was not zero only for eye positions to one side of straight ahead gaze.
9. Motor learning caused many FTNs to become strongly modulated when the monkey tracked a target that moved exactly with him during head rotation. When the gain of the VOR was low, FTNs showed increased firing during head motion away from the side of the recording. When the gain of the VOR was high, many FTNs showed increased firing during head motion toward the side of the recording.
10. T. Langer, A. F. Fuchs, M. C. Chubb, C. A. Scudder, S. G. Lisberger, *J. Comp. Neurol.* **235**, 26 (1985).
11. Details of the method for converting the digital train of action potentials into an analog record related to firing rate are in (4).
12. It would have been difficult to measure response latency from FTNs recorded when the gain of the VOR was low, because the responses were too small to allow accurate estimates of latency.
13. We are assuming that FTNs are in VOR pathways and project to motoneurons because (i) FTNs are inhibited by stimulation of the flocculus and (ii)

- studies in nonprimate species have shown that the flocculus inhibits direct brain stem VOR pathways [S. M. Highstein, *Exp. Brain Res.* **17**, 301 (1973); M. Ito, N. Nisimaru, M. Yamamoto, *ibid.* **24**, 257 (1976); W. Precht and R. Baker, *ibid.* **14**, 158 (1972)].
14. D. A. Robinson, *J. Neurophysiol.* **38**, 393 (1970).
15. S. G. Lisberger and A. F. Fuchs, *ibid.* **41**, 733 (1978); F. A. Miles, J. H. Fuller, D. J. Braitman, B. M. Dow, *ibid.* **43**, 1437 (1980).
16. L. S. Stone and S. G. Lisberger, *Neurosci. Lett.* **72**, 163 (1986).
17. Our recordings during rapid changes in head velocity agree with previous data (6).
18. It was not practical to measure PC response latency before motor learning, because PC firing rate normally shows very little modulation of firing rate during the VOR.
19. We thank D. Belknap, F. Miles, M. Stryker, and R. Nicoll for helpful criticism of earlier versions of the manuscript. Supported by EY03878 from the National Institutes of Health, BNS 8444605 from the National Science Foundation, a Scholars Award from the McKnight Foundation, and a Development Award from the McKnight Neuroscience Endowment Fund.

25 July 1988; accepted 7 October 1988

Spatially Resolved Calcium Dynamics of Mammalian Purkinje Cells in Cerebellar Slice

DAVID W. TANK, MUTSUYUKI SUGIMORI, JOHN A. CONNOR, RODOLFO R. LLINÁS

Microfluorometric imaging was used to study the correlation of intracellular calcium concentration with voltage-dependent electrical activity in guinea pig cerebellar Purkinje cells. The spatiotemporal dynamics of intracellular calcium concentration are demonstrated during spontaneous and evoked activity. The results are in agreement with hypotheses of dendritic segregation of calcium conductances suggested by electrophysiological experiments. These in vitro slice fluorescence imaging methods are applicable to a wide range of problems in central nervous system biochemical and electrophysiological functions.

THE SPATIAL DISTRIBUTION OF IONIC channels over the plasmalemma and the associated compartmentalization of the integrative and the cell biological properties is a critical issue in the characterization of central neuronal function. The locus specificity of the synaptic input may influence both the electrical integrative properties of the cell and the degree of precision with which different compartments may be regulated biochemically. For example, the spatial distribution of second messenger systems activated by Ca^{2+} will be determined by ionic channel distribution.

The nature of the distribution of voltage-dependent ionic channels over the somatic

and dendritic membranes of neurons has been investigated often in recent years (1). Segregation of the voltage-dependent Na^+ and Ca^{2+} ionic conductances was hypothesized when intradendritic recordings from Purkinje cells in avian cerebellum (2) and mammalian cerebellar slices in vitro (3) demonstrated the presence of voltage-dependent Ca^{2+} conductances capable of generating dendritic spikes. The results from such studies suggested that in this cell Ca^{2+} conductance is most prominent, if not exclusively present, in the dendritic tree, and the voltage-dependent Na^+ conductance is restricted to the soma and axon (3). Furthermore, electrophysiological examination of the slow Ca^{2+} -dependent potentials and regenerative spikes (3) suggested that the ionic conductances underlying these two distinct components might also be spatially separated within the dendritic tree. The experiments presented here were designed

REFERENCES AND NOTES

1. E. L. Keller, *Vision Res.* **18**, 311 (1978).
2. The characteristics of motor learning have been studied in a number of species. For monkeys, see F. A. Miles and B. B. Eighmy [*J. Neurophysiol.* **43**, 1406 (1980)].
3. S. G. Lisberger, *Science* **225**, 74 (1984).
4. _____ and T. A. Pavelko, *J. Neurosci.* **6**, 346 (1986).
5. S. G. Lisberger, F. A. Miles, D. S. Zee, *J. Neurophysiol.* **52**, 1140 (1984).
6. E. Watanabe, *Brain Res.* **297**, 169 (1984); F. A. Miles, D. J. Braitman, B. M. Dow, *J. Neurophysiol.* **43**, 1477 (1980).

D. W. Tank and J. A. Connor, Molecular Biophysics Research Department, AT&T Bell Laboratories, Murray Hill, NJ 07974.
M. Sugimori and R. R. Llinás, Department of Physiology and Biophysics, New York University School of Medicine, New York, NY 10016.

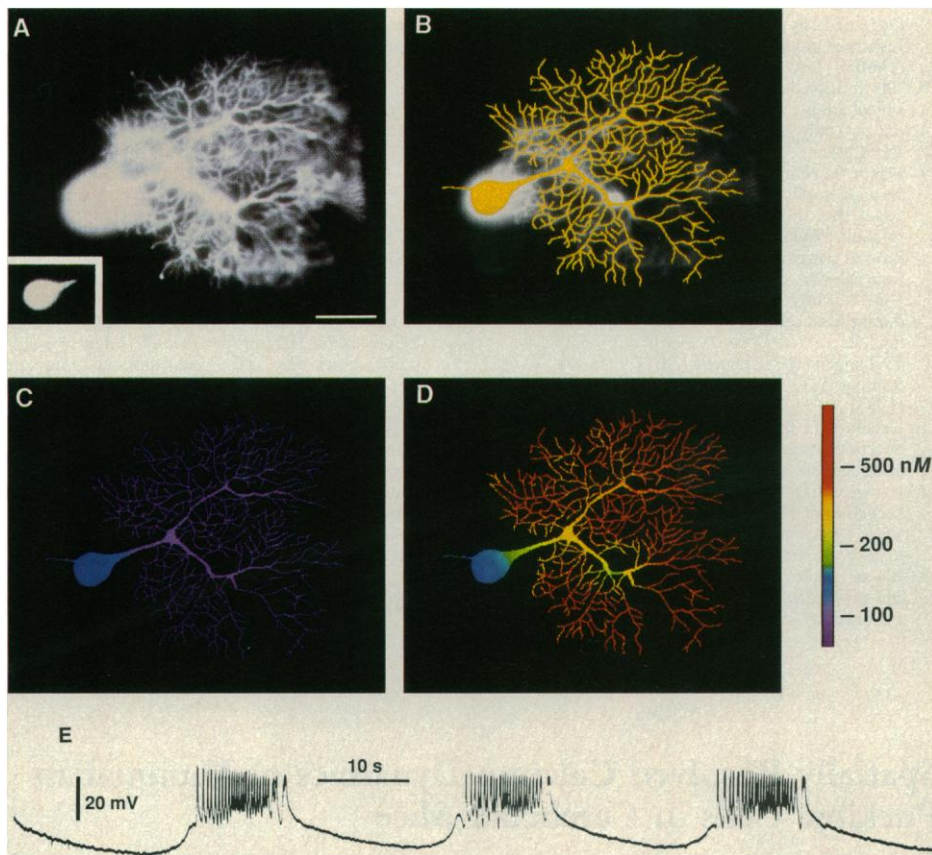


Fig. 1. (A) High-resolution fluorescence image of a Purkinje cell filled with fura-2 by microinjection (380-nm excitation). The relation between fluorescence intensity and position on the gray scale of the figure was reduced by approximately tenfold in the somatic region (inset) to clearly show the cellular boundaries. The scale bar represents 50 μm . The cellular boundaries from 380-nm excited fluorescence images were used to define a mask (B) (in yellow), that defined the fluorescent areas of the images where ratios and the associated $[\text{Ca}^{2+}]_i$ were subsequently computed. (C) Map of $[\text{Ca}^{2+}]_i$ during the period of electrical quiescence. (D) Map of $[\text{Ca}^{2+}]_i$ during the peak of the $[\text{Ca}^{2+}]_i$ accumulation. (E) Spontaneous electrical oscillations recorded from this cell during the indicator loading period.

to map the location of voltage-dependent Ca^{2+} channels as inferred from the specific regions of the neuron where intracellular calcium concentrations, $[\text{Ca}^{2+}]_i$, underwent the greatest changes as a result of electrical activity and to establish the speed with which $[\text{Ca}^{2+}]_i$ can be buffered within the cytoplasm.

Spatial distributions of $[\text{Ca}^{2+}]_i$ in Purkinje cells in cerebellar slices from adult guinea pigs were determined from the ratio of digital microfluorometric images of intracellular fura-2 excited at 340 and 380 nm (4) and correlated with cell electrical activity. Individual cells were filled with the fluorescent Ca^{2+} indicator fura-2 (5) by iontophoresis after intrasomatic or intradendritic microelectrode penetrations. Injected cells had a fluorescence image (Fig. 1A) similar to that observed for Lucifer yellow-injected cells. The fura-2 filled the entire dendritic arbor and appeared uniformly distributed within the cytoplasm. Compartmentalization or dye aggregation was never observed. Cell electrical activity was elicited by intracellular microelectrode current injection or,

for most results, electrical activity occurred spontaneously in the form of oscillation (Fig. 1E). As previously described (3), this oscillatory behavior is characterized by periods of complex spike activity lasting for 10 to 15 s that alternated with periods of silence of approximately equal duration. These spontaneous oscillations are generated by intrinsic voltage-dependent Ca^{2+} conductance changes, as demonstrated by the ineffectiveness of the Na^+ conductance blocker tetrodotoxin to modify the cell's behavior and by the blockage of oscillations after the administration of Ca^{2+} conductance blockers (3).

Intradendritic $[\text{Ca}^{2+}]_i$ increased 10- to 100-fold between the inactive and active phases of oscillation, whereas somatic levels remained largely unchanged. This is illustrated in the high resolution (300 by 500 pixels) maps in Fig. 1. Figure 1B shows a computer-generated mask that covers the brightly fluorescent areas of the image in Fig. 1A. In the highly fluorescent areas of the image covered by the mask, ratios of fluorescence excited by 340- and 380-nm

incident light and the associated $[\text{Ca}^{2+}]_i$ were computed from image pairs taken during the silent and active phases of oscillation. Figure 1C shows the $[\text{Ca}^{2+}]_i$ distribution during the silent period of the oscillation cycle. Calcium levels are low ($<60 \text{ nM}$) throughout the cell, with the distal dendritic branches slightly lower than the soma. Figure 1D shows the $[\text{Ca}^{2+}]_i$ distribution during the active period of oscillation, where the dendrites, especially the finer branches, display high $[\text{Ca}^{2+}]_i$ with respect to the soma and the axon. Recordings in which both electrical activity and $[\text{Ca}^{2+}]_i$ were followed simultaneously (4) showed the unique correspondence between the spontaneous discharge and elevated $[\text{Ca}^{2+}]_i$ in the dendritic regions.

The spatiotemporal dynamics of $[\text{Ca}^{2+}]_i$ during an oscillatory cycle were measured by sequential fluorescence-image acquisition. The spatial detail of Fig. 1 was made possible by the sacrifice of time resolution; each exposure in the image pairs lasted 5 s. This caused the measured peak of the $[\text{Ca}^{2+}]_i$ transient to be blunted because of time averaging and prevented a study of the kinetic changes of $[\text{Ca}^{2+}]_i$ during the cycle. With reduced spatial resolution (125 by 175 pixels), frame pairs were taken every 2 s. Dendrite fine structure was lost but pictures were acquired and stored fast enough to show the $[\text{Ca}^{2+}]_i$ dynamics during a spontaneous cycle (Fig. 2). The beginning (Fig. 2A) of the continuous sequence (Fig. 2, A to H) shows $[\text{Ca}^{2+}]_i$ at its lowest and most uniform. The next three panels, taken consecutively, follow the $[\text{Ca}^{2+}]_i$ to, and past, its maxima. It is clear that small dendrites are the first to undergo a $[\text{Ca}^{2+}]_i$ increase and that the changes are the largest at those sites. By contrast, the $[\text{Ca}^{2+}]_i$ in the soma changed very little ($<50 \text{ nM}$) and with appreciable delay, whereas the axon remained very low throughout the cycle. At the peak of the measured response there was a $>300 \text{ nM}$ $[\text{Ca}^{2+}]_i$ gradient between the dendritic tree and the soma. In some experiments, $[\text{Ca}^{2+}]_i$ in the small dendrites reached levels that saturated the fura-2 response, that is, to levels >3 to $4 \mu\text{M}$. At the time the $[\text{Ca}^{2+}]_i$ map of Fig. 2F was made, $[\text{Ca}^{2+}]_i$ in the small dendrites had been nearly restored to ground state but concentrations in the primary and secondary dendrites were considerably higher (this effect is even more apparent in the map of Fig. 2M). This probably reflects a different time course for the activation of the Ca^{2+} channels in this region. Because of the short diffusion distances involved, this region should have lost the excess $[\text{Ca}^{2+}]_i$ to the surrounding tertiary dendrites by the time the measurement was made. Figure 2G shows the completion

of the oscillation cycle. When the $[Ca^{2+}]_i$ of representative sections of distal dendrite, primary dendrite, soma, and axon are plotted for each time point (Fig. 2Q), the increases in dendritic $[Ca^{2+}]_i$ and the phase lead of distal dendritic $[Ca^{2+}]_i$ changes over primary dendrites and soma are clearly observed. In addition to the large $[Ca^{2+}]_i$ gradients that developed during the active phase, the small dendrites recovered rapidly. Generally, the $[Ca^{2+}]_i$ went from near maximum ($>1 \mu M$) to resting level ($<75 nM$) within 2 s, which suggests the presence of efficient Ca^{2+} buffering systems in these

dendrites, and indicates a close relation between the site and duration of voltage-dependent Ca^{2+} conductance increases and the fluorescent signal. Under our experimental conditions, Purkinje cells continued to oscillate for 2 to 3 hours after impalement. During this time the sequence of the events accompanying each oscillatory phase and the distribution of $[Ca^{2+}]_i$ from one oscillatory event to the next was almost identical. Similar spatiotemporal patterns of Ca^{2+} concentration during complete oscillations (for example, see Fig. 2, I to P) were obtained in six different neurons.

Consistent with previous electrophysiological experiments (6), application of a fraction of funnel web spider venom (FTX) blocked both spontaneous electrical oscillations and the oscillations in $[Ca^{2+}]_i$ concentration. This toxin is a specific blocker of voltage-dependent Ca^{2+} channels in central neurons (6). After toxin administration (4), a total blockage of oscillation was observed after 5 min. The blockage continued for a period of 20 to 30 min during continuous perfusion of toxin-free saline. During this period, constant low levels of $[Ca^{2+}]_i$ were maintained in both soma and dendritic regions for up to 30 min after the toxin was applied.

During spontaneous oscillations in non-toxin-treated cells we always observed higher concentrations of Ca^{2+} in the initial (thick) section of the primary dendrite than in the soma or axon. These results are most

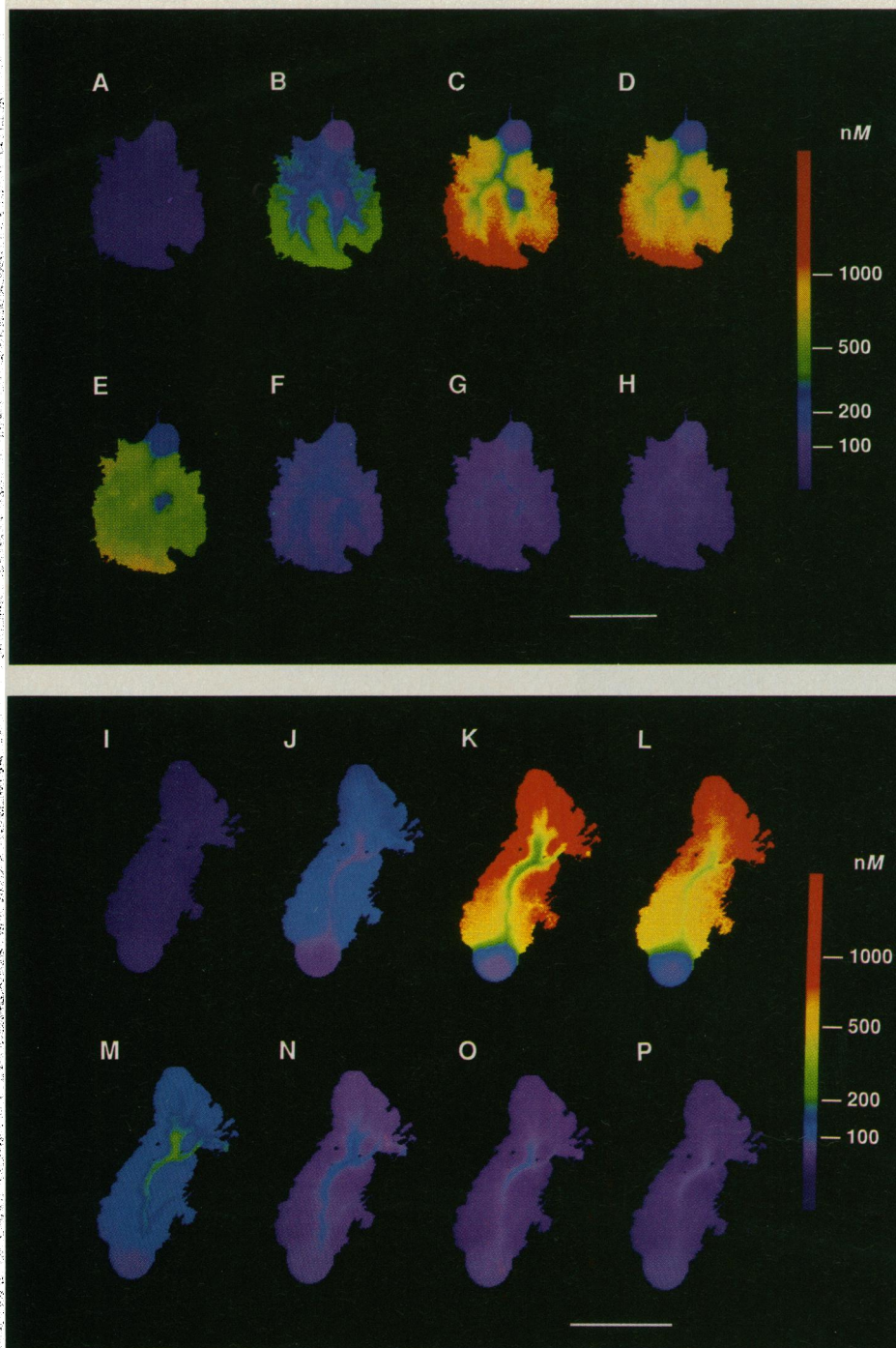


Fig. 2. (A to H) Calcium distributions during one cycle of spontaneous oscillation. Images were sequentially acquired at higher rates (one pair every 2.0 s) but at lower spatial resolution (125 by 175 pixels) for the same Purkinje cell shown in Fig. 1. Calcium levels in the distal tertiary dendrites peak at an earlier phase of the oscillation (C) than the primary and secondary main dendrite (D). In (H) the $[Ca^{2+}]_i$ distribution has returned to that typical of the quiescent periods [compare to the period of spontaneous oscillation (Fig. 1E)]. The dynamics were similar in all cells measured. (I to P) The spatiotemporal pattern of $[Ca^{2+}]_i$ distribution in a different Purkinje cell under identical conditions are shown. In (M), the lag phase of Ca^{2+} response in the primary dendrite is apparent. (Q) Calcium levels at four cellular locations during the sequence of $[Ca^{2+}]_i$ dynamics shown in (A to H). The large rapid Ca^{2+} flux into the fine dendrites (\circ) is followed by a delayed but substantial rise in the primary dendrite (Δ) and a modest rise in the soma (\square). The level of $[Ca^{2+}]_i$ in the axon (∇) remains very low. The scale bars represent 50 μm .

easily explained by a strong gradient of Ca^{2+} conductance along the proximal dendrite-soma axis, but we cannot rule out the possibility of nonuniform buffering capacity as a contributing factor to the $[\text{Ca}^{2+}]_i$ gradients in all cases. Where depolarizing current was applied through a microelectrode in the soma, we were able to demonstrate nonuniform increases in $[\text{Ca}^{2+}]_i$ along the proximal dendrite. Figure 3 shows one such example in which $[\text{Ca}^{2+}]_i$ was measured at a hyperpolarized membrane potential (Fig. 3A) and during the 1.2-s period after a step of depolarizing current. In such instances, differences in buffer capacity caused by surface to volume differences are minimal and the nonuniform $[\text{Ca}^{2+}]_i$ changes would have to reflect localized influx or internal partitioning of buffering elements in the dendrite.

Our results represent a direct demonstration of the dendritic localization of voltage-dependent Ca^{2+} channels in Purkinje cells and are in substantial agreement with measurements of Ross and Werman (7), which showed dendritic Ca^{2+} influx with arsenazo III absorption. Our findings extend the spatial resolution of these measurements and show the involvement of the fine dendrite structure. The large signal-to-noise ratios we have observed and the absence of any detectable phototoxicity indicate that with suitable modifications of imaging equipment, high-

resolution images of intracellular ion concentrations will also be possible at much higher temporal resolution.

In addition to illustrating the use of the fura-2 imaging technique in the analysis of in situ adult central neurons, our results demonstrate the presence of distinct dynamic patterns in the $[\text{Ca}^{2+}]_i$ distribution during central nervous system neuronal firing. Our results also suggest that the early-phase Ca^{2+} conductances are spatially located in the tertiary branches of the dendritic tree, with further invasion of the main dendrites occurring as a secondary event. We suggest that the activity of these two different dendritic segments corresponds to the two different types of electroresponsiveness originally reported for Purkinje cells (3). Indeed, physiologically the initial phase of dendritic activation is characterized by a slow Ca^{2+} -dependent depolarization, which reaches a plateau and is followed by powerful all-or-none Ca^{2+} -dependent dendritic spikes. The results presented here are in agreement with the hypothesis that the slow first component of the response is produced by voltage-dependent Ca^{2+} conductance in the tertiary branches, whereas the large spike component arises in the primary and secondary dendritic tree. The possibility that, in addition to spatial segregation, these two distinct Ca^{2+} conductances are subserved by

two distinct voltage-dependent Ca^{2+} channels requires further study. Indeed, some of the differences observed may arise from the absence of fast K^+ conductances in the fine dendritic branches, in addition to spatial differences in channel density.

The physiological implications of the findings presented here are significant to the understanding of Purkinje cell integration. We propose that because of the tertiary branch Ca^{2+} electroresponsiveness, synaptic input from the parallel fibers to the spines in the tertiary branchlets would be enhanced in such a way that neuronal integration in the primary branches was not altered. When the activity in the tertiary branches becomes great enough, full Ca^{2+} -dependent dendritic spikes would be generated by the main dendritic tree. Conversely, after activation of a climbing fiber, which is known to produce full dendritic spikes at its initial phase, a full dendritic spike would be generated at the main dendritic tree, where the climbing fiber is actually in contact with the Purkinje cell (8). After this initial dendritic spike, the secondary plateau potential, which characterizes climbing fiber activation, would be generated. Thus the distribution of Ca^{2+} conductance over the dendritic tree is ultimately tuned for a degree of electrophysiological sophistication suggested by its quasi-baroque morphology.

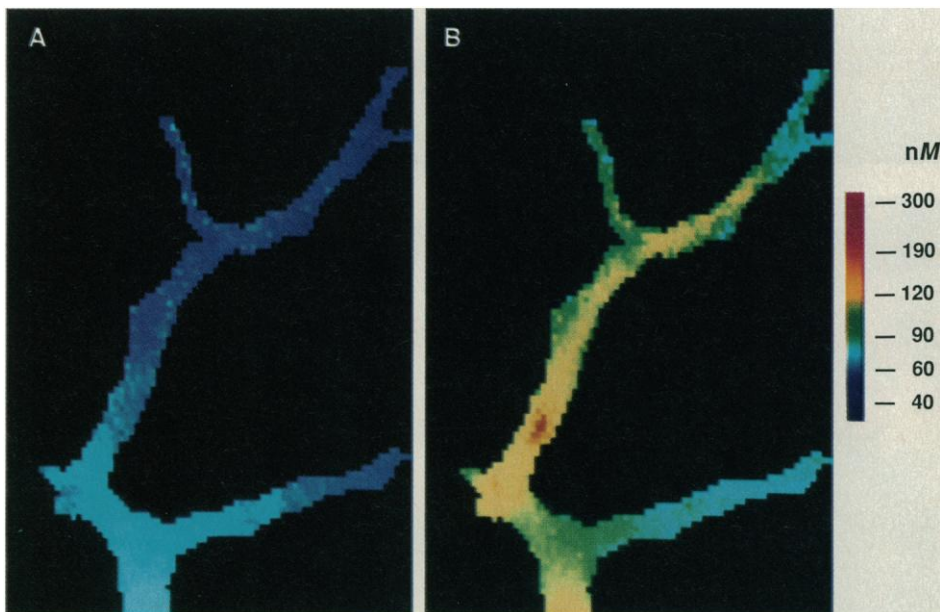


Fig. 3. $[\text{Ca}^{2+}]_i$ distribution in a primary dendrite during a quiescent period observed during hyperpolarizing current injection at the soma (A) and during the initial 1.2 s of depolarizing current to the soma (B) that evoked a brief train of spikes (0.2 s) followed by subthreshold depolarization. The "hot spot" in the lower left of (B) represents a 70 to 80 nM differential of $[\text{Ca}^{2+}]_i$ when compared to the surrounding yellow shaded areas. This response was tested with two to three different stimulus periods to verify the constant location of the nonuniformities. The difference in the ratio values for these two regions was 35%. Noise variations were less than 5%. It was not possible to deliver enough current through the microelectrodes to drive the cells into sustained oscillations or spiking and thus the relative lack of response in the upper and right-hand sections of dendrite possibly reflects electrical propagation failure. Image dimension: 50 by 75 μm .

REFERENCES AND NOTES

1. W. E. Crill and P. C. Schwindt, *Trends Neurosci.* **6**, 236 (1983); R. Llinás, in *Brain Slices*, R. Dingle, Ed. (Plenum, New York, 1984), pp. 7-24.
2. R. Llinás and R. Hess, *Proc. Natl. Acad. Sci. U.S.A.* **73**, 2520 (1976).
3. R. Llinás and M. Sugimori, *J. Physiol. (London)* **305**, 175 (1980); *ibid.*, p. 197.
4. Guinea pig cerebellar slices were obtained by standard procedures (3). During experiments, slices were continuously perfused with saline of the following composition: 124 mM NaCl; 5 mM KCl; 1.2 mM KH_2PO_4 ; 2.4 mM CaCl_2 ; 1.3 mM MgSO_4 ; 26 mM NaHCO_3 ; and 10 mM glucose, equilibrated with 95%/5% O_2/CO_2 . The slice chamber temperature was maintained at 32°C. Preparations routinely maintained spontaneous activity for 2 to 3 hours. Two experimental configurations were used for microfluorometric imaging: (i) cells from slices of 250 μm thickness were viewed and impaled from above on the stage of an upright microscope (Zeiss UEM); (ii) cells (from slices of 150 μm thickness) were viewed from below and impaled from above with an inverted microscope (Zeiss IM-35). In both cases, Purkinje cells were injected with microelectrodes pulled from 1.5-mm tubing (#6030 AM Systems), containing a 10 mM solution of the K^+ salt of fura-2 (5) (Molecular Probes) in 100 mM KCl (electrode resistance: 60 to 80 megohm). Iontophoretic current (-1 to -2 nA) was passed continuously during the filling period (10 to 15 min), except for brief periods of interruption when spontaneous electrical activity was measured (Neuro Data IR-283). In some experiments FTX, isolated in our laboratories, was added to the chamber upstream from the slice, to a final estimated concentration of ~10 nM. For experiments with the upright microscope, the microelectrode was removed for precision optical measurements because of the short working distance of

the objective (Nikon UVF 10 objective, covered with Saran Wrap for water immersion use) and the preference for penetrating the cells at a 45° angle to the plane of the slice. In the inverted configuration (Nikon UVF-20 objective) the electrode was left in the cells and we monitored electrical activity during optical measurements. Generally, optical resolution was reduced in the inverted microscope as a result of light scattering in the tissue, because injected cells were not usually near the optical surface. However, in the few injected cells that were located near the bottom of the slice, optical resolution improved. With the exception of Fig. 3, A and B, all figures in this report were made from images acquired on the upright microscope. Both microscopes were fitted with cooled charge-coupled device (CCD) cameras (Photometrics, model 220 on the UEM, model 80

on the IM35) with computer-controlled data acquisition. The $[Ca^{2+}]_i$ was determined from images at 340- and 380-nm excitation by using the ratio method (5). Details of data acquisition, background subtraction, calibration, and other experimental considerations have been given elsewhere [J. A. Connor, *Proc. Natl. Acad. Sci. U.S.A.* **83**, 6179 (1986)]. Reported Ca^{2+} levels assumed a viscosity correction corresponding to a 30% reduction in the 340-nm/380-nm fluorescence ratio [——, P. E. Hockberger, H. Y. Tseng, *J. Neurosci.* **7**, 1384 (1987); M. Poenic, J. Alderton, R. Steinhart, R. Y. Tsien, *Science* **233**, 886 (1986)]. CCD camera exposure times were 5 s for each fluorescent image used to produce the maps in Fig. 1, 0.9 s for the images in Fig. 2, and 250 ms for the images in Fig. 3. Frame pairs were separated by <0.5 s.

- G. Gryniewicz, M. Poenic, R. Y. Tsien, *J. Biol. Chem.* **260**, 3440 (1985).
- M. Sugimori and R. Llinás, *Soc. Neurosci. Abstr.* **13**, 228 (1987). In earlier work, FTX was referred to as ATX (*Agelenopsis Aperta toxin*).
- W. N. Ross and R. Werman, *J. Physiol. (London)* **389**, 319 (1986).
- C. F. Ekerot and O. Oscarsson, *ibid.* **318**, 207 (1981).
- Supported by AT&T Bell Laboratories, NS-13742 from the National Institute of Neurological and Communicative Disorders and Stroke (NINCDS), F49620 from the Air Force Office of Scientific Research (AFOSR), and Fidia Corporation.

23 June 1988; accepted 3 October 1988

Growth and Transparency in the Lens, an Epithelial Tissue, Stimulated by Pulses of PDGF

BARBARA BREWITT* AND JOHN I. CLARK

The rat lens undergoes dramatic growth during early postnatal development. Lens weight increased by a factor of 23 in 26 days. Growth rate per day oscillated between 0 and 87 percent. A new culture system was designed to study the oscillations in growth during development. Lens growth and transparency in vitro required pulsatile delivery of platelet-derived growth factor (PDGF) in HL-1 serum-free medium. Continuous delivery of HL-1 medium with PDGF or pulsatile delivery of HL-1 medium without PDGF resulted in lens opacity and no growth. These results provide direct evidence that PDGF stimulates an epithelial tissue and that oscillations in growth occur during normal development of the rat lens.

THE RAT LENS IS AN IDEAL MODEL for studies of normal growth and development of an epithelial tissue (1). In the embryo, an invagination of surface ectoderm results in the formation of a lens vesicle (2). The lens becomes a solid cellular tissue, without vessels and nerves, when the posterior epithelial cells elongate to fill the vesicle. The anterior epithelial cells migrate laterally, elongate, and differentiate into mature lens fibers, which constitute the body of the lens. An unusual feature of the lens is that the apical surfaces of the epithelial cells face inward and attach to lens fibers (2). The outside of the lens is covered by a thick basement membrane, the lens capsule, that influences the elastic, nutritional, and transport properties of the lens. All nutrients for normal growth and development come from the surrounding aqueous and vitreous fluids and pass through the lens capsule.

A high concentration of protein is required if the mammalian lens is to function as a transparent, refractile optical element (3). The lack of blood vessels and nerves in the lens is consistent with the general classification of an epithelial tissue and is neces-

sary for transparency. Numerous gap junctions allow intercellular transport of the ions and small molecules required for lens growth (2).

External factors that may regulate lens growth include insulin-like growth factor, fibroblast growth factor, and epidermal growth factor, which are thought to be present in the surrounding aqueous and

vitreous humors (4–6). These factors have been tested in lens epithelial cell culture and may act alone (4, 6) or synergistically (5). Growth factors may be responsible for major changes in transparency, hydration, wet and dry weights, protein content, gene expression, and cell shape that occur during the first 30 days of postnatal rat lens development (2, 7, 8). Despite many attempts at lens organ culture under conditions that would permit the identification and isolation of regulatory factors, an ideal culture medium for normal lens development has not yet been identified (5, 9). Cultured lenses typically lose transparency and have lower rates of mitosis and protein synthesis than are found in vivo (9). No culture systems are known to be suitable for studies of the development of lens transparency. Our goal was to develop an in vitro system for studies of external factors that regulate lens growth during the development of transparency.

A systematic evaluation of changes in wet and dry weights during normal develop-

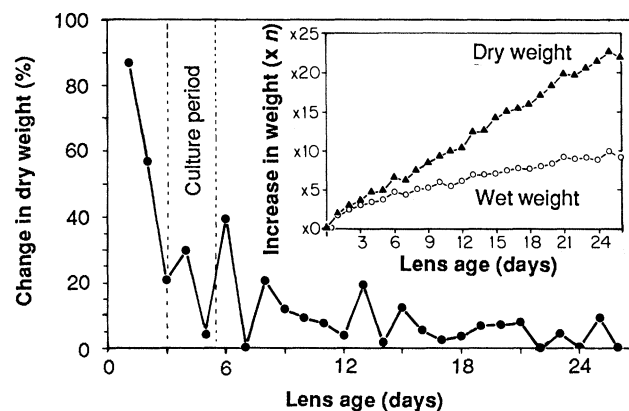


Fig. 1. In vivo lens development. Rates of increase in dry weight oscillated between 0 and 87% per day. Dry and wet weights increased by factors of 23 and 10, respectively, between birth and 26 days (inset). The y-axis in the inset indicates multiples of birth-weight. Ten to 27 nonlittermate rats were killed, at each age. We avoided diurnal effects by conducting all experiments between 1 and 3 p.m. After enucleation, lenses were removed by pos-

terior cuts through the retina. Wet and dry weights were measured on an electrical analytical balance (Mettler AE163). Lenses were dried at 80°C to constant weight. The time period selected for organ culture is shown by the vertical dashed lines. The percent change in dry weight was calculated by the formula $(DW_{x+1} - DW_x)/DW_x \times 100$ where DW_{x+1} is lens dry weight on day $x + 1$ and DW_x is lens dry weight on the previous day. The standard error is contained within the symbols in both plots. Instead of growing continuously (21), the lens showed large oscillations during neonatal development.

Department of Biological Structure, University of Washington, School of Medicine, Seattle, WA 98195.

*To whom correspondence should be addressed.